Data in Brief 34 (2021) 106676

Contents lists available at ScienceDirect

Data in Brief

journal homepage: www.elsevier.com/locate/dib

Data Article

Dataset on fractographic analysis of various SiC-based fibers

S. Mazerat, R. Pailler*

Univ. Bordeaux, CNRS, CEA, SAFRAN CERAMICS, LCTS, UMR 5801, F-33600 Pessac, France

ARTICLE INFO

Article history:
Received 17 November 2020
Revised 11 December 2020
Accepted 16 December 2020
Available online 24 December 2020

Keywords:
SiC fiber
Fractographic analysis
Toughness
Mirror

ABSTRACT

This data article reports a systematic fractographic analysis of SiC-based filaments aiming at stress intensity factors assessment. A total of 11 fiber types (as-received or chlorinated Nicalon® and Tyranno® of all three generations) where therefore repeatedly tensile tested to generate the fracture surfaces. The tensile strengths were found to be independent to defect location (surface or internal). The well-known linear square root dependence of strength on mirror, mist or hackle outer radius was reaffirmed. These measurements reveal some residual tensile stresses on Nicalon® fibers, statement however questioned by the broad data scattering. Moreover, it is shown the surface etching treatment didn't affected (generating or releasing) such residual stress. A null *y*-intercept was consequently adopted to assess the characteristic stress intensity factors (K_{IC}, mirror, mist or hackle constants). The toughness (K_{IC}) estimated this way ranges from 1.0 to 1.9 MPa $m^{1/2}$ and shows a clear dependency to substrate composition: higher values were extracted on oxygen-free fibers. The A_m/K_{IC} ratio, estimated to equal 1.8 and independent to substrate type, is a key parameter that would assist further fractographic investigations.

* Corresponding author.
E-mail address: pailler@lcts.u-bordeaux.fr (R. Pailler).

https://doi.org/10.1016/j.dib.2020.106676

Specifications Table

Subject	Material Science
Specific subject area	Tensile testing and subsequent fractographic analysis of SiC-based fiber.
Type of data	Table Figure
How data were acquired	SEM observation were performed on the fracture surface of filaments after their tensile fracture.
Data format	Raw and analyzed
Parameters for data collection	Different types of SiC-based fibers, 11 in total brought to 17 including different batches and surface etched, were tensile tested to determine their tensile strength and observe the fracture pattern. Tensile tests were performed in the same conditions (0.5% min^{-1}).
Description of data collection	Prior to any test, a layer of paraffin grease was deposited on the filament probe to rescue the fragments. These fragments were washed in acetone, mounted on brass plate and observed with SEM. The fracture pattern was systematically observed concentric to the flaw: mirror, mist, hackle and branching regions.
Data source location	Univ. Bordeaux, CNRS, CEA, SAFRAN CERAMICS, LCTS, UMR 5801, F-33600 Pessac, France
Data accessibility	All data herein and supplementary file are available within this article.
Related research	F. Teyssandier, G. Puyoo, S. Mazerat, G. Chollon, R. Pailler, F. Babonneau, Contribution to the understanding of the microstructure of first generation Si-C-O fibers, in: M. Halbig, S. Mathur, T. Ohji, M. Singh (Eds.), Advanced Processing and Manufacturing Technologies for Structural and Multifunctional Materials VI, 33 (2012) Ceram. Eng. Sci. Proc. Wiley, New York pp. 1–11. In Press doi:10.1002/9781118217528.ch1

Value of the Data

- This dataset is valued because it comprises significant amount of fracture pattern analysis for various SiC based fibers. Stress intensity factors for mirror, mist and hackle regions (Am, Ah and Ab) were estimated.
- The toughness estimates extracted from this work can further be used for any theory based on fracture mechanics law.
- The data presented herein can assist the analysis of fracture surface when the actual tensile strength of each filament can not be assessed, i.e. of a composite containing several hundred of filaments for instance.
- Toughness and its relationship to mirror radius was assessed for each fiber type.
- Stress intensity factors identified 3 fiber families, dependent on their oxygen and carbon free contents.

1. Data Description

Continuous fine SiC-based fibers have been, and continue to be, of great interest for demanding applications thanks to their low density, high strength, high thermal conductivity, chemical inertness and stability at elevated temperatures. The microstructure of these fibers consists of SiC grains in the nanometer range, embedded in a continuum of silicon oxycarbide (SiCO) and carbon free (C_{free}). The volume fraction of this continuum, affecting the microstructure and filament properties, is dependent on manufacturing process parameters (precursor, curing atmosphere, pyrolysis temperature) [1]. A total of 13 batches of fibers covering a broad range of composition, microstructure and properties were investigated: extending from the first SiCO (Nicalon® NL101, NL102, NL207, Tyranno® Grade S (TS or TS11), Lox-M, ZMI, ZM), the second (Hi-Nicalon®, Lox-E, ZE, AM) to the third generation (Hi-Nicalon® Type S). In addition, surface etched fibers from a previous work [2] were added to answer the following question: could such treatment affecting positively the tensile strength somehow generate or release residual stresses? Their fracture pattern, typical for brittle material, is characterized by mirror, mist, hackle and branching regions concentric to the flaw as shown on Fig. 1.

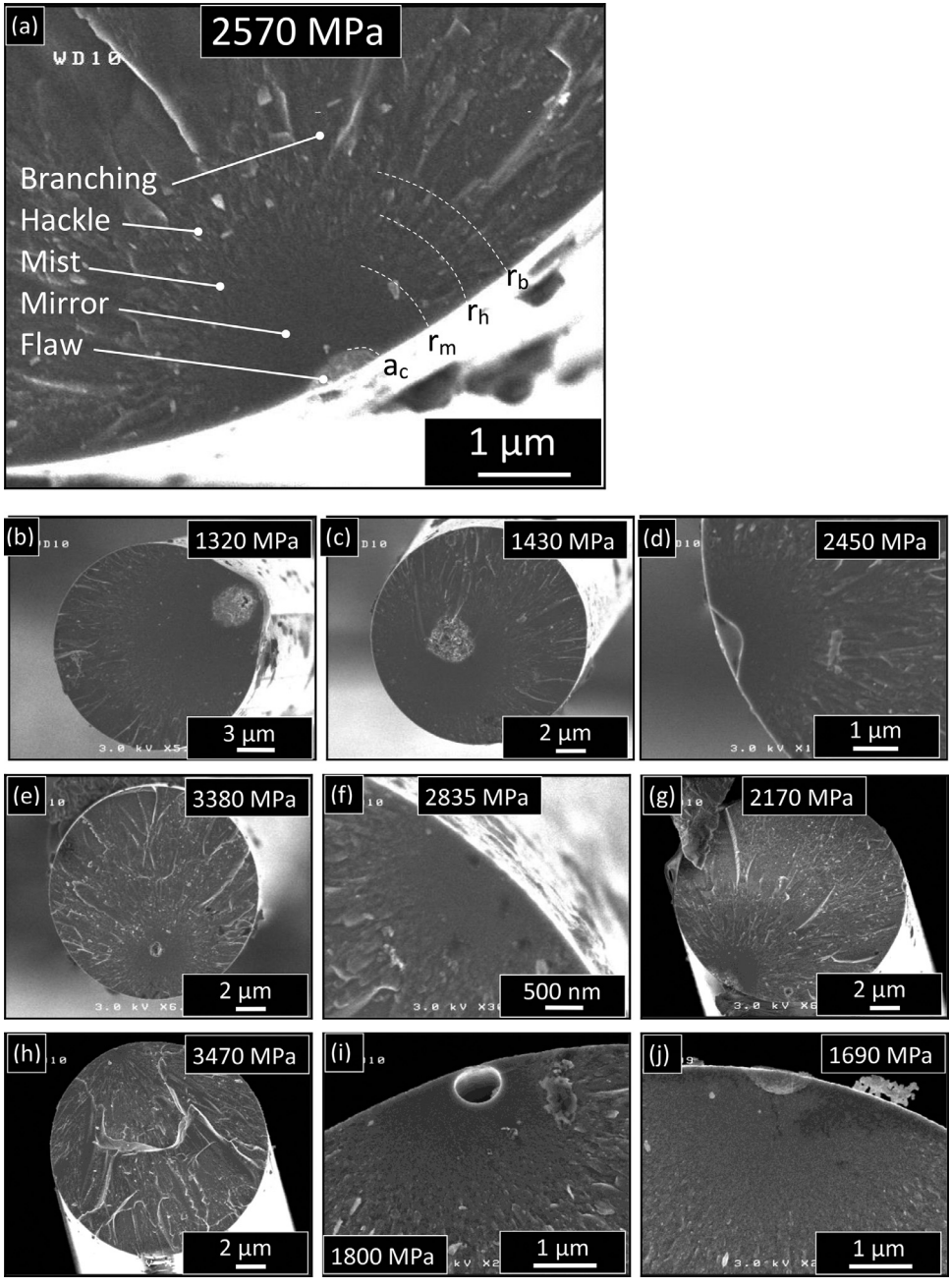

Fig. 1. Typical fractography of SiC-based fibers showing the typical fracture pattern: (a-d). NL101, (e). Hi-Ni, (f). NL102, (g-k). NL207, (l). TS, (m). TS11, (n). Lox-M, (o). ZM, (p,q). Lox-M etched over 550 nm.

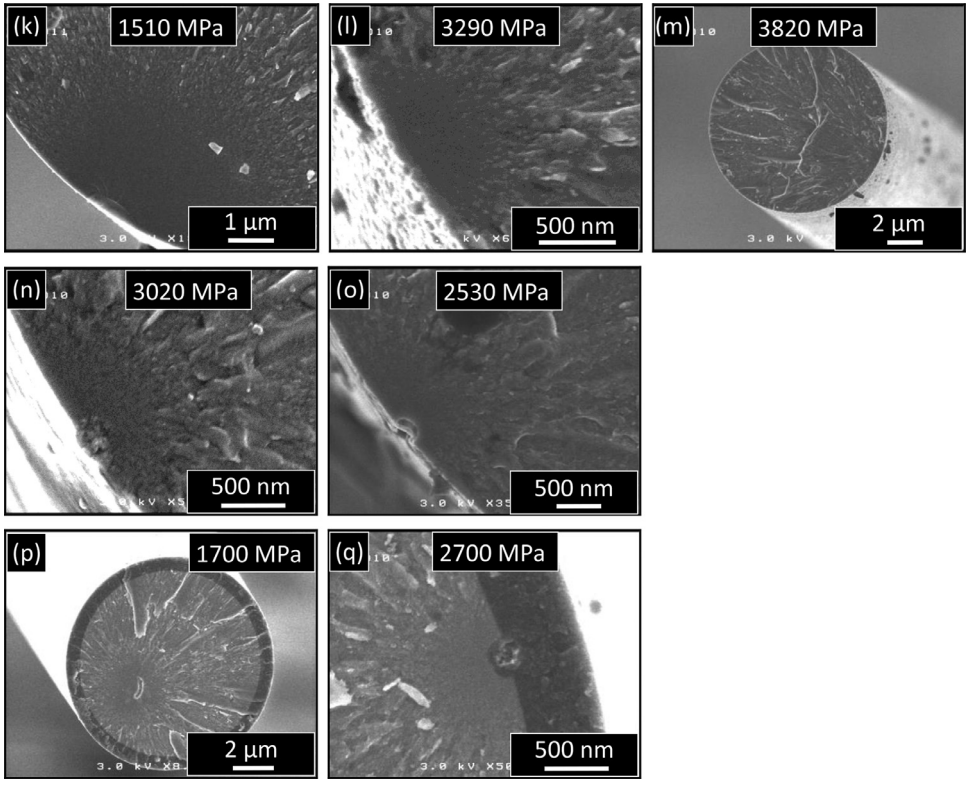

Fig. 1. Continued

As a pre-requisite to such analysis, fact all defect types lead to strength belonging to one single population (no multimodal Weibull distribution (Eq. (1)) [3]) was confirmed on Nicalon NL207 and Hi-Ni (Fig. 2) [4]. When the critical flaw is surface located, no tendency to lower tensile strength can be noticed. Toughness was estimated from the relationship between the tensile strength and the inverse square root of defect size (a_c), limited to semi-circular (penny) shape crack (only 15–40% of the flaws concerned [1,2]). This latter restriction was motivated by fact the geometry factor (Y, Eq. (6)) for other flaw types (internal, heterogeneity…) is unknown. Values for K_{IC} obtained by linear regression ranges from 1 to 1.9 MPa $m^{1/2}$ (Fig. 3, Table 1) in good agreement with literature data on such samples [5,6]. As expected, K_{IC} is dependent on fiber composition and microstructure (Fig. 4). When oxygen free (Hi-Ni-S, Hi-Ni and ZE), a K_{IC} larger than 1.2 MPa $m^{1/2}$ was calculated whereas this value is lower in presence of SiCO glassy phase (>5at.% O) [7]. Oxygen rich fibers can further be classified in two families. The first one gathers ZMI, ZM, Lox-E with $K_{IC} = 1.0$ MPa $m^{1/2}$ and display a percolated carbon free network [8] contrary to the second group composed of NL101, NL102, NL207, TS, TS11, Lox-M, AM with $K_{IC} = 1.1–1.2$ MPa $m^{1/2}$.

Radii separating the different regions surrounding the flaw were also identified (r_m r_h and r_b respectively the outer limit for mirror, mist and hackle). The linear relationship between tensile strength and the inverse square root of these radii was confirmed. The ordinate of such relationship can be used to reveal tensile or compressive residual stress Eq. (8)). On this basis, some authors reported residual compressive stresses of 280 MPa on Nicalon® [9]. A converse tendency, rather tensile residual stress of approximately 200–350 MPa at the surface and 600–700 MPa internally, seems here highlighted on the same fiber type (Fig. 5). However, given

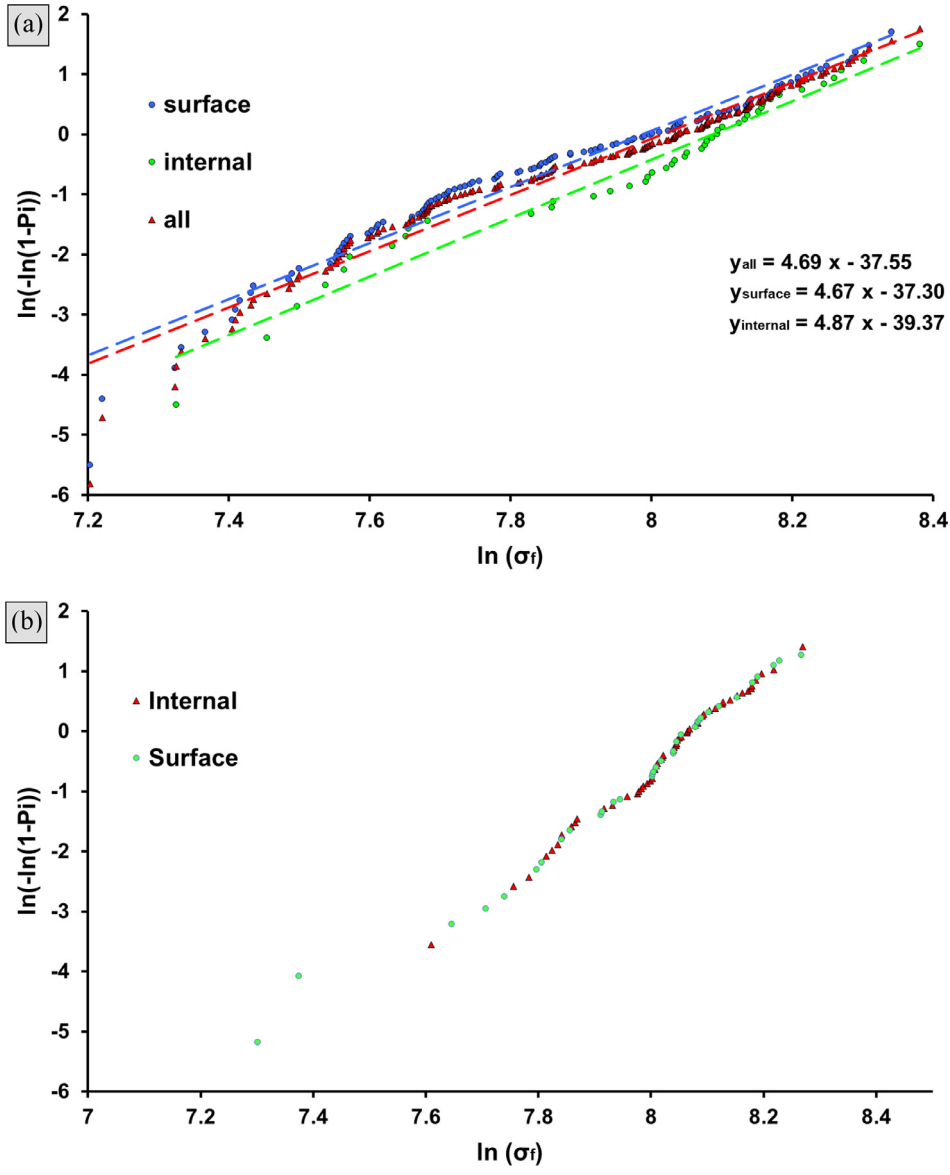

Fig. 2. Weibull distribution plot for (a). Nicalon NL207 or (b). Hi-Ni fiber strengths identifying the flaw positioning (surface of internally located).

the broad measurement scattering, such observation could be questioned, hence the decision to take a null ordinate (Eqs. (3)–((5)) and to neglect such residual stresses in the following analysis (Figs. 6). Raw data of flaw, mirror, mist, hackle and branching radii with associated tensile strengths are reported in the Supplementary File 1. Analysis of surface etched samples (chlorination treatment) followed the same trend, thus did not highlighted stress release. Mirror constants (A_m) lying between 1.6 and 3 MPa $m^{1/2}$ were this way assessed in agreement with literature data [9-11]. The mist (A_h) and hackle (A_b) constants respectively range from

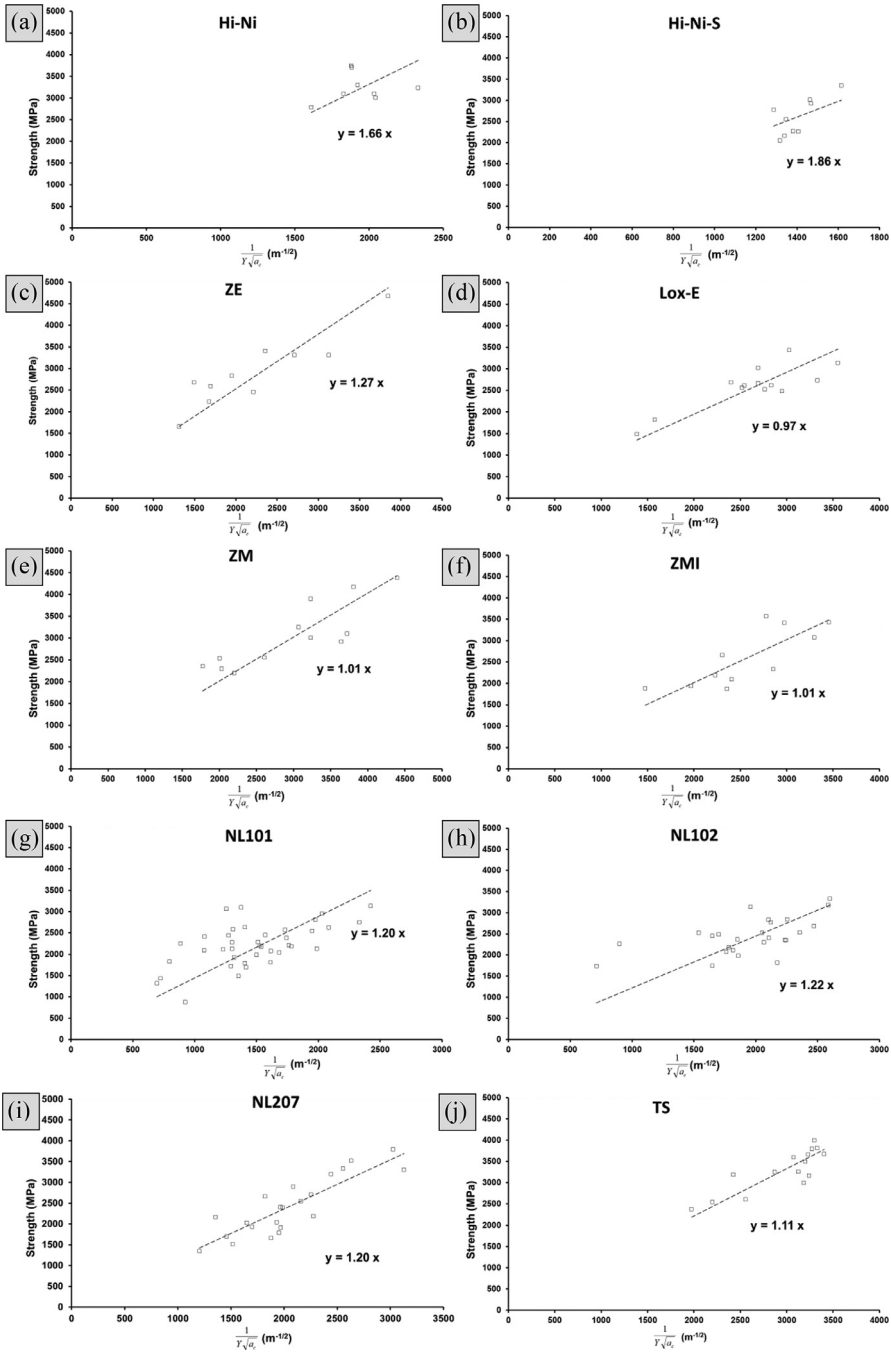

Fig. 3. Failure stress versus reciprocal square root of crack length ($a_c^{-1/2}$) of various SiC-based fibers: (a). Hi-Ni, (b). Hi-Ni-S, (c). ZE, (d). Lox-E, (e). ZM, (f). ZMI, (g). NL101, (h). NL102, (i). NL207, (j). TS, (k). TS11, (l). Lox-M, (m). AM.

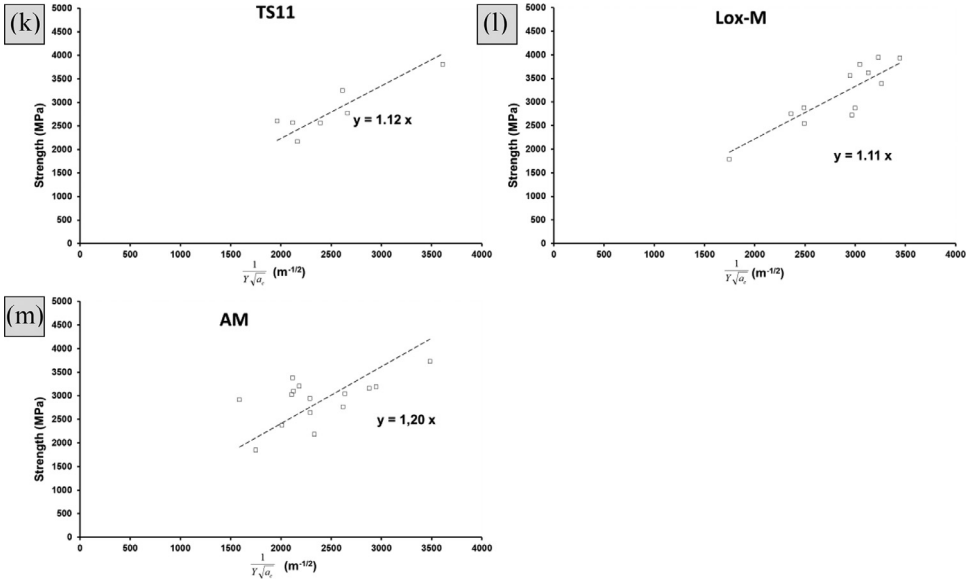

Fig. 3. Continued

Table 1
Summary of data extracted from fractograhic analysis for SiC-based fibers.

	σ_f (MPa)	K_{IC} (MPa m$^{1/2}$)	A_m	A_h	A_b	$\frac{A_m}{K_{IC}}$	$\frac{A_h}{K_{IC}}$	$\frac{A_b}{K_{IC}}$
Hi-Ni	3140	1.66	2.93	3.62	4.69	1.77	2.18	2.83
Hi-Ni-S	2880	1.86	2.63	3.71	4.64	1.41	1.99	2.49
ZE	3250	1.27	2.25	2.78	3.57	1.77	2.19	2.81
Lox-E	2940	0.97	1.82	2.24	2.82	1.88	2.31	2.91
ZM	3440	1.01	1.94	2.51	3.30	1.92	2.49	3.27
ZMI	3080	1.01	1.85	2.25	2.97	1.83	2.23	2.94
NL101	2170	1.20	2.40	2.75	3.43	2.00	2.29	2.86
NL102	2560	1.22	2.37	2.69	3.31	1.94	2.20	2.71
NL207	2840	1.20	2.37	2.82	3.32	1.98	2.35	2.77
TS	3150	1.11	1.68	1.95	2.50	1.51	1.76	2.25
TS11	2780	1.12	2.00	2.53	2.99	1.79	2.26	2.67
Lox-M	2980	1.11	1.94	2.26	2.88	1.75	2.04	2.59
AM	2810	1.20	2.00	2.33	2.99	1.67	1.94	2.49

2 to 3.7 MPa m$^{1/2}$ and from 2.5 to 4.7 MPa m$^{1/2}$. Likewise above observation on toughness, these stress intensity constants can be related to fiber chemical composition: when oxygen free (<5at.%) A_m >2.4 MPa m$^{1/2}$ A_h >2.7 MPa m$^{1/2}$ and A_b >3.4 MPa m$^{1/2}$ (ZE not following systematically this rule), whereas the same constants for oxygen containing fibers and non-percolated C_{free} led to A_m 1.9–2.4 MPa m$^{1/2}$, A_h 2.2–2.7 MPa m$^{1/2}$, A_b 2.9–3.4 MPa m$^{1/2}$. In presence of percolated carbon free phase, these coefficients fall to 1.9, 2.2 and 2.8–2.9 MPa m$^{1/2}$ respectively. If TS11 fiber follows this trend, TS (8.5 µm mean diameter, non percolated carbon network) seems however to detach with smaller stress intensity values, despite identical toughness.

It should be emphases–18 these constants are proportional to K_{IC} (Fig. 19), which means the flaw size is proportional to characteristic radii. On this basis, B_m, the ratio between A_m and K_{IC}

Table 2
Tensile strength and associated mirror radius for some fibers presenting internal or surface located flaws.

Surface located σf.f (MPa)	r_m (nm)	Internal located σf.f (MPa)	r_m (nm)
1344	3242	1726	3691
1515	2495	1802	1113
1695	1402	1927	1437
1789	1239	1942	2157
1904	1019	2064	2566
1912	1174	2104	2387
1936	1771	2111	1654
2122	1268	2169	1315
2141	1359	2588	1663
2157	1630	2592	1003
2169	1217	2812	790
2182	788	2844	875
2233	1306	2890	753
2255	1395	2932	640
2334	820	2956	735
2395	757	2965	1157
2405	980	2984	1265
2474	1108	3045	524
2525	781	3068	904
2550	1024	3080	929
2578	763	3126	639
2591	614	3135	935
2737	743	3202	661
2772	754	3204	551
2823	522	3216	752
2880	816	3274	627
2900	681	3277	965
2951	467	3296	617
3078	482	3376	564
3098	542	3403	540
3198	560	3470	1071
3226	432	3486	560
3364	401	3489	969
3410	443	3491	748
3423	439	3532	578
3482	587	3576	517
3528	723	3691	437
3635	529	3809	678
3672	398	3865	387
3741	452	3904	521
3965	367	4030	516
4058	398	4362	422

(Eq. (7)), extends from 1.4 to 2.0 with a 1.8 mean value, independent to the fiber type. This value contrast with the 2.35 often considered in literature [9,12]. The same concept is true for mist and hackle regions, with A_h/K_{IC} and A_b/K_{IC} equal to 2.2 and 2.7 respectively (Table 1). It is worthwhile noting the outer delimitation of mist and hackle regions is often more straightforward and reliable than mirror-mist boundary. These results can assist the fractographic analysis of here studied SiC-based fibers. By extension, the relationship between stress intensity factors and composition would give some guidelines to estimate properties of alternative fibers. The tendency to lower toughness of SiCO substrates which display a percolated C_{free} network could be the object of future investigations.

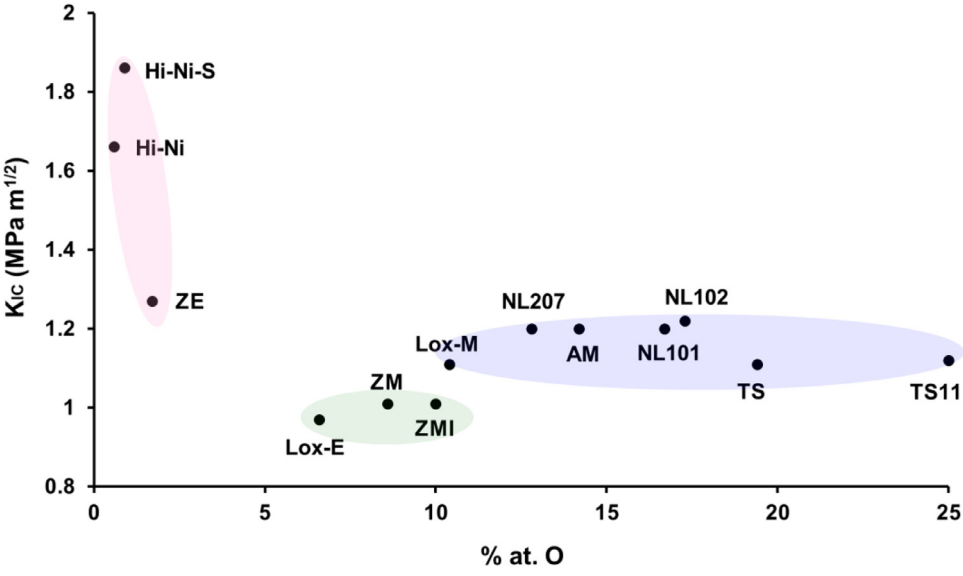

Fig. 4. Toughness versus oxygen content (given in [1]) for the different SiC-based fibers here studied, highlighting different behaviors.

2. Experimental Design, Materials and Methods

2.1. Material

Three generations of SiC-based fibers are commercially available, synthesized by the conversion of polycarbosilane and commercialized by Nippon carbon Co. Ltd. or UBE Industries Ltd. In this dataset, 7 first-generation (oxygen cured) fibers are reported: Nicalon® NL100, Nicalon® NL207, Tyranno® Grade S, referred as TS, Tyranno® Lox-M, Tyranno® ZMI, Tyranno® ZM and Tyranno® AM. Hi-Nicalon (named Hi-Ni), Tyranno® Lox-E and Tyranno® ZE belongs to the second-generation (electron beam cured) whereas Hi-Nicalon Type S (named Hi-Ni-S) is a third generation (high temperature annealing) SiC-based fiber completing the work. Two different batches of NL100 (NL101 and NL102) and TS (TS and TS11, with 8.5 and 11 µm respective diameters) were characterized, bringing to 13 the total number of fiber types. Their chemical compositions can be found in the corresponding works [1] and [13]. Some chlorinated tows were also examined. These samples were desized by heat treatment at 650 °C for 10 min in air followed by thin silica film removal in 10 vol.% hydrofluoric acid bath for 4 min, dried and then treated under pure chlorine at intermediate temperature. Treatments, with duration and temperature dependent on substrate type [13], resulted in a homogeneous surface transformation into a carbide derived carbon phase [8] erasing or blunting surface located flaws [2].

2.2. Method

Mechanical properties of filaments were measured at room temperature in ambient atmosphere on a dedicated tensile machine. Single filaments were randomly pulled out from a tow, mounted, aligned and glued on a paper holder with 25 mm window. The diameter of each sample was then measured using its laser diffraction pattern. Once gripped in the device, a layer

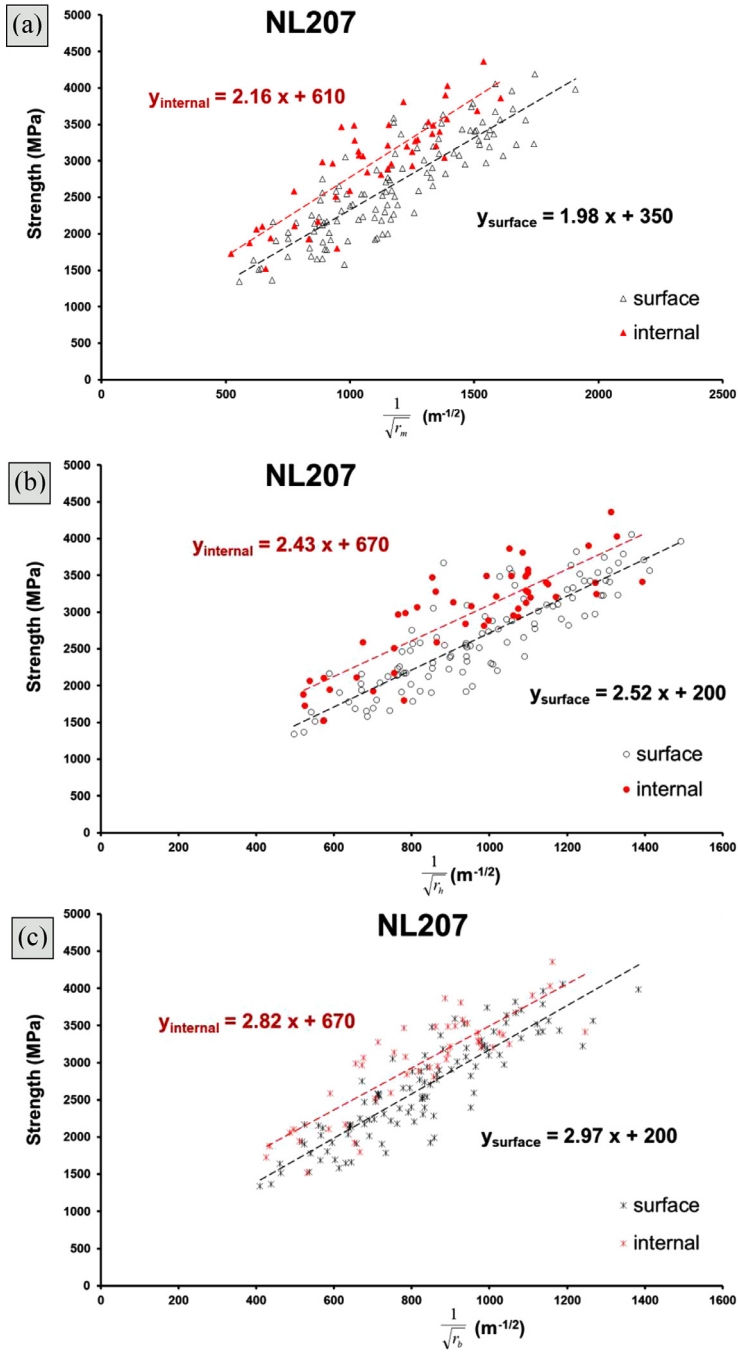

Fig. 5. Tensile strength vs. (a). mirror (b). mist (c). hackle outer radius for NL207 revealing residual tensile stresses of 200–350 MPa on the surface and 610–670 MPa internally.

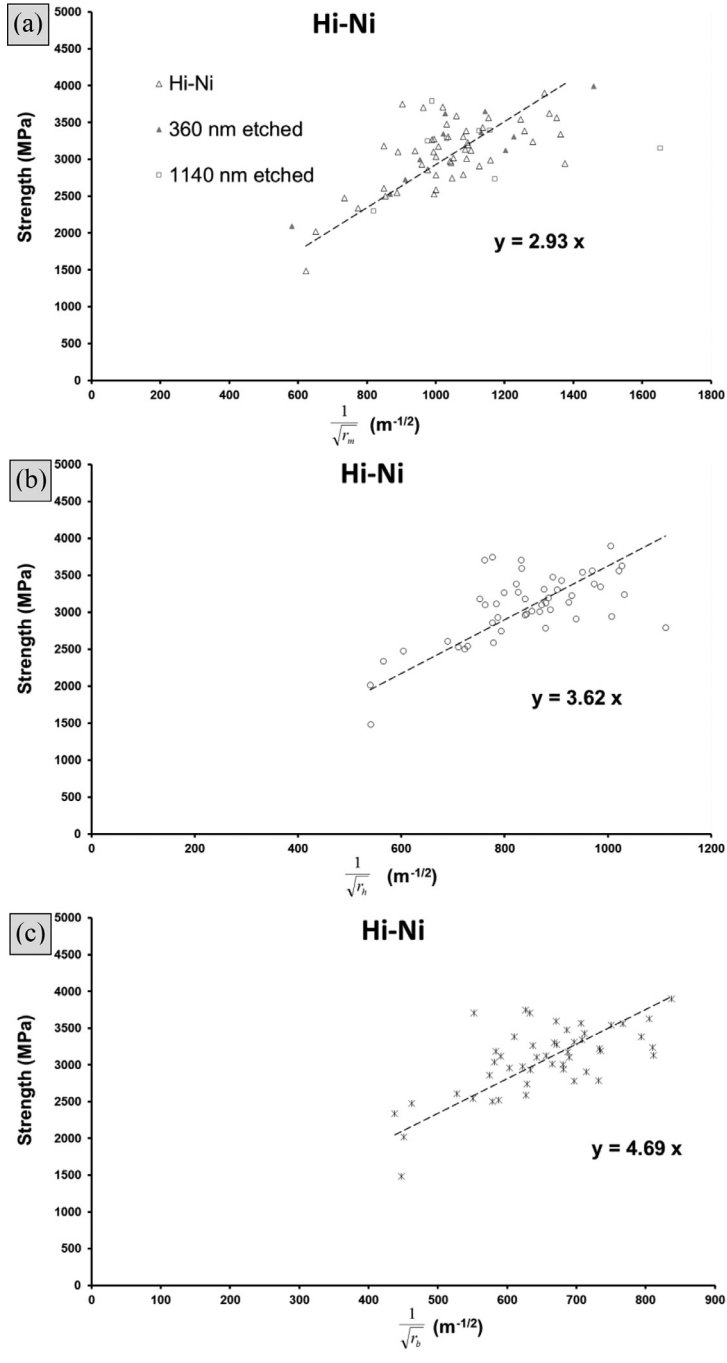

Fig. 6. Tensile strength vs. reciprocal square root of (a). mirror (b). mist (c). hackle outer radius for Hi-Ni fibers. Data for chlorinated Hi-Ni over 360 or 1140 nm are also given.

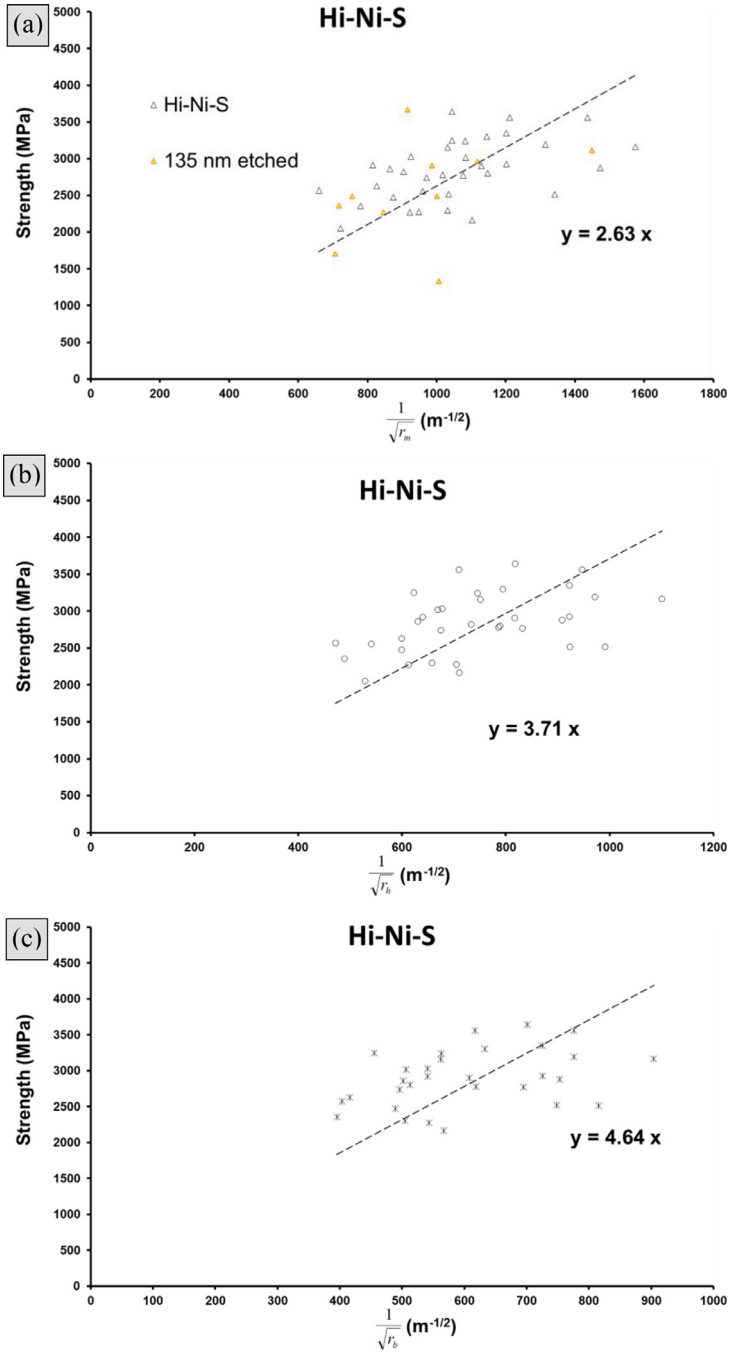

Fig. 7. Tensile strength vs. reciprocal square root of (a). mirror (b). mist (c). hackle outer radius for Hi-Ni-S fibers. Data for chlorinated Hi-Ni-S over 130 nm are also given.

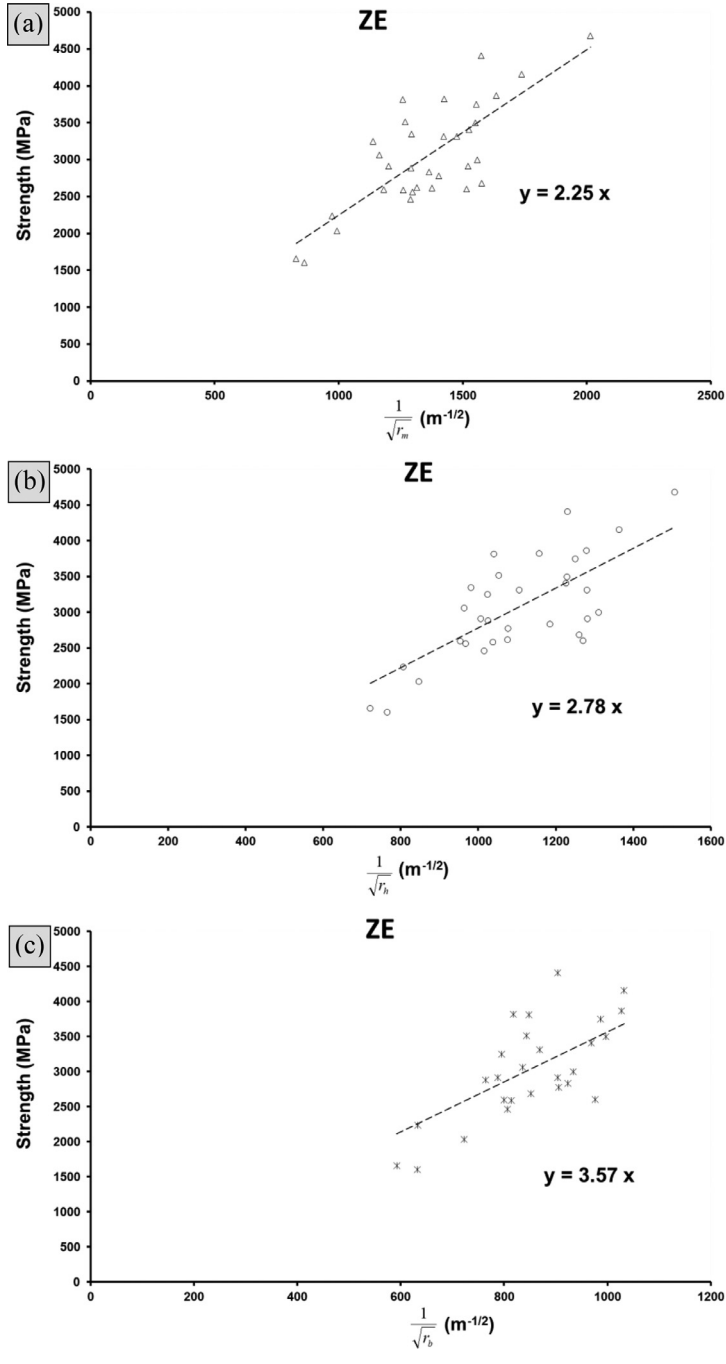

Fig. 8. Tensile strength vs. reciprocal square root of (a). mirror (b). mist (c). hackle outer radius for ZE fibers.

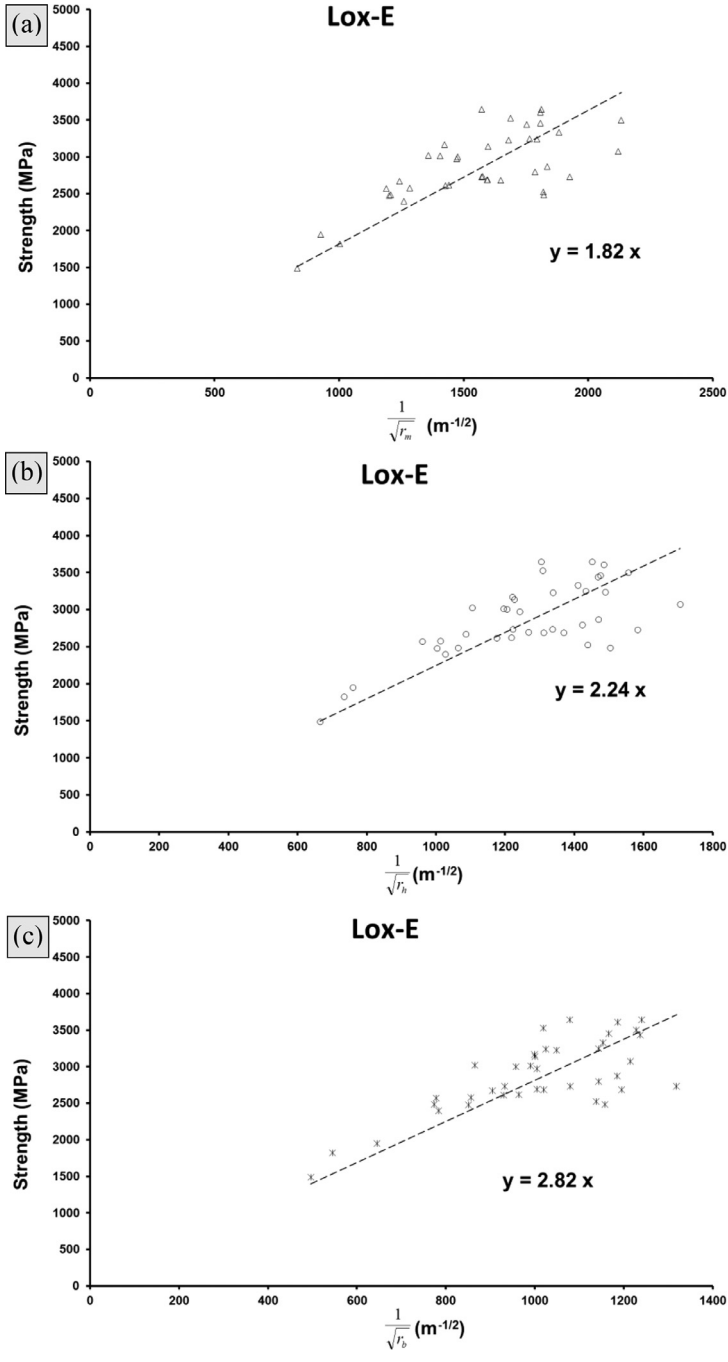

Fig. 9. Tensile strength vs. reciprocal square root of (a). mirror (b). mist (c). hackle outer radius for Lox-E fibers.

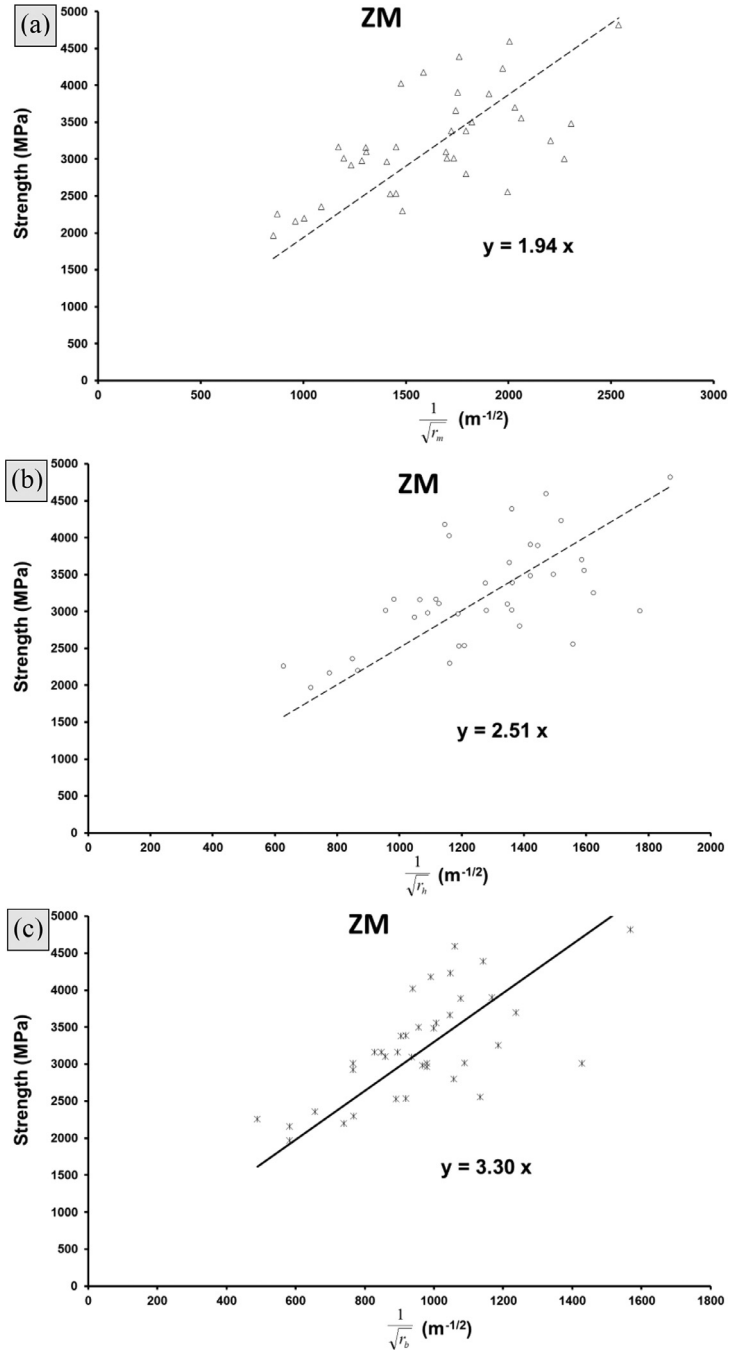

Fig. 10. Tensile strength vs. reciprocal square root of (a). mirror (b). mist (c). hackle outer radius for ZM fibers.

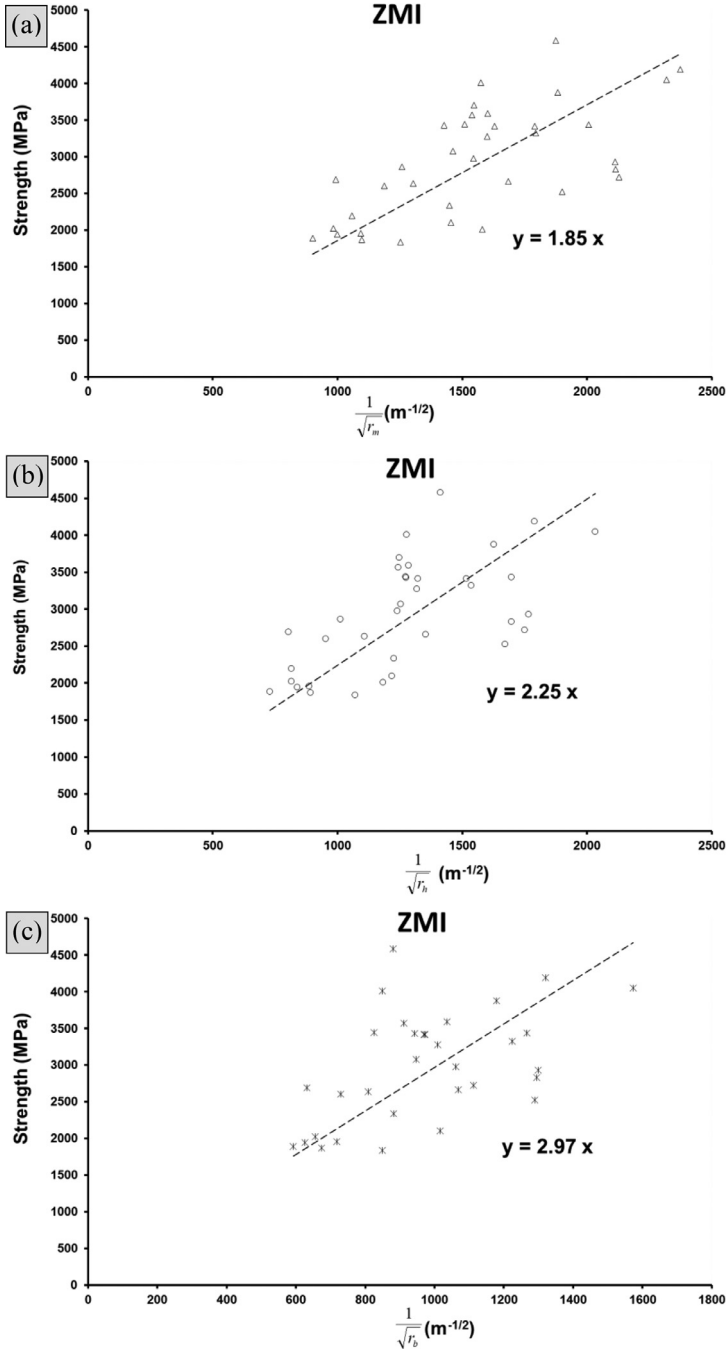

Fig. 11. Tensile strength vs. reciprocal square root of (a). mirror (b). mist (c). hackle outer radius for ZMI fibers.

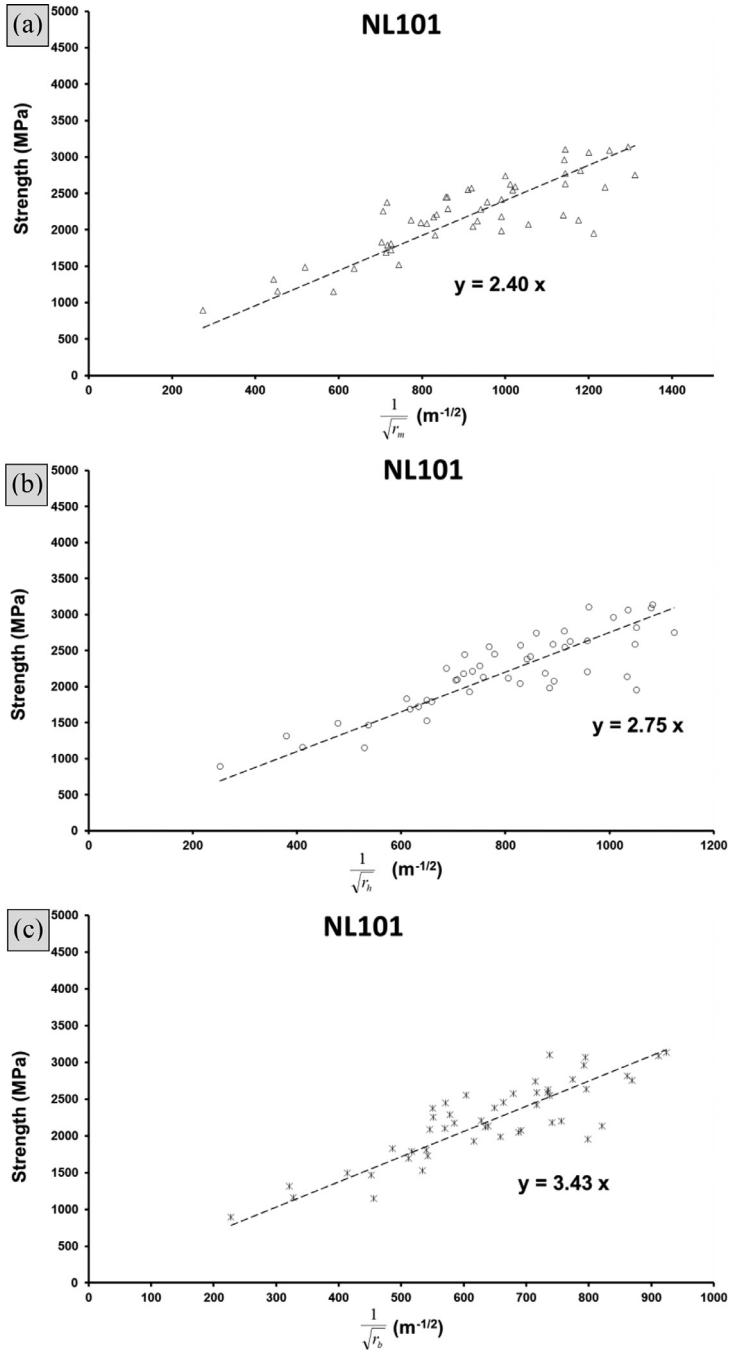

Fig. 12. Tensile strength vs. reciprocal square root of (a). mirror (b). mist (c). hackle outer radius for NL101 fibers.

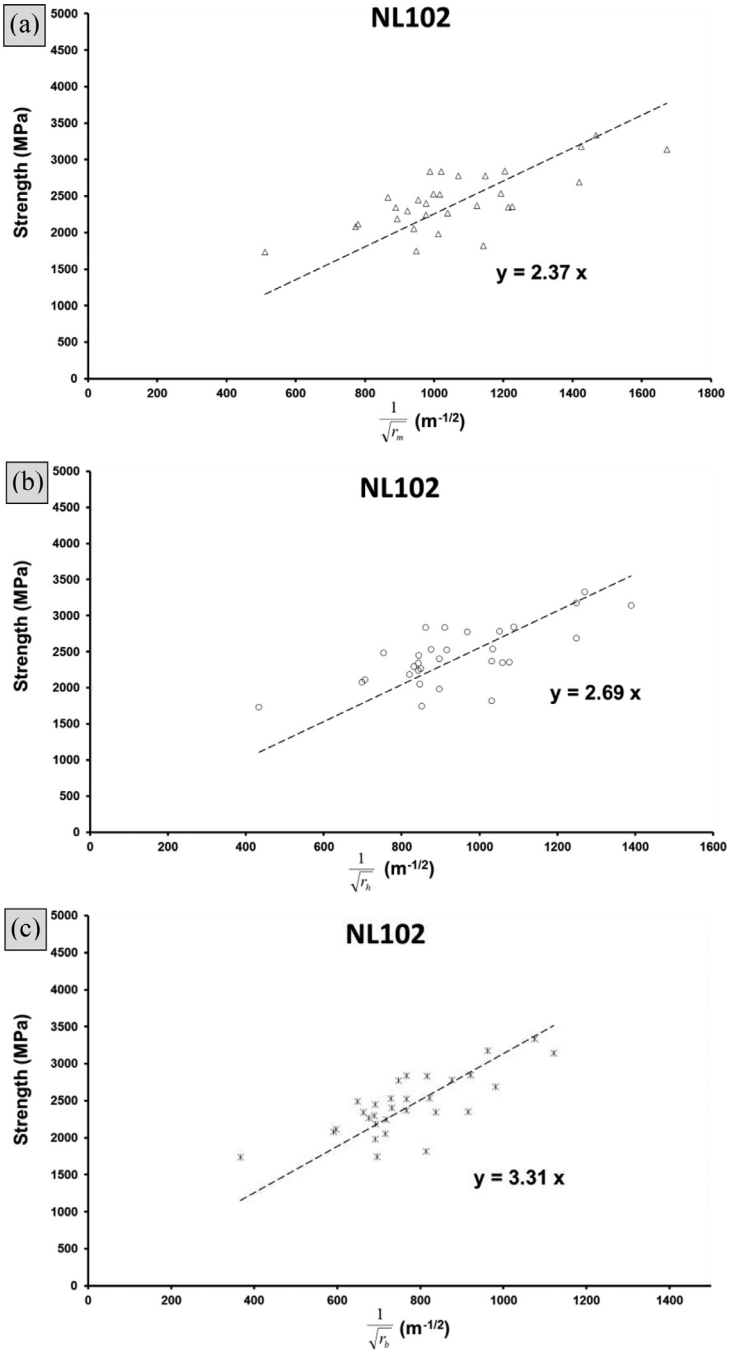

Fig. 13. Tensile strength vs. reciprocal square root of (a). mirror (b). mist (c). hackle outer radius for NL102 fibers.

of paraffin grease was deposited on the probe to rescue the fiber fragments [3] and the paper holder cut on both sides. Tensile tests were carried at a constant cross-head rate of 0.5% mm^{-1}, measured by a LVDT extensometer mounted on the grips. The distribution of tensile strength (σ_f) was interpreted using a single modal Weibull model given in Eq. (1). This distribution assumes flaws randomly dispersed in the tested volume.

$$P_i = 1 - e^{-\left(\frac{\sigma_f}{\sigma_1}\right)^m} \tag{1}$$

$$P_i = \frac{i - 0.5}{N} \tag{2}$$

Where P_i is the probability of i^{th} ranked σ_f strength (Eq. (2)), N the total number of specimens, σ_1 the Weibull characteristic strength corresponding to a 37% survival probability and m the Weibull modulus.

Fiber fragments were subsequently recovered, washed in acetone, mounted on brass plate and observed with SEM (S4500 from Hitachi). The classical fracture pattern was analyzed for each section (Fig. 1) [14], identifying regions delimited by following radii:

- r_m the limit between mirror and mist regions;
- r_h the limit between mist and hackle regions;
- r_b the limit between hackle and branching regions.

The relationship between strength and inverse square root of the mirror radius [15–18], with A_m a material constant (Eq. (3)), is well established. The same exists for mist (Eq. (4)) or hackle (Eq. (5)) outer radii defining A_h and A_b constants, however seldom reported.

$$\sigma_f = \frac{A_m}{\sqrt{r_m}} \tag{3}$$

$$\sigma_f = \frac{A_h}{\sqrt{r_h}} \tag{4}$$

$$\sigma_f = \frac{A_b}{\sqrt{r_b}} \tag{5}$$

Another remarkable and meaningful information is the size of the flaw that caused the failure. When penny shaped, its radius (a_c) is also related to the tensile strength Eq. (6)). Y is the geometry factor ($2\ \pi^{-1/2}$) for this defect type and K_{IC} the toughness. Large uncertainty for flaw size assessment (commonly few tens of nm for SiC-based fibers) and limited fraction of penny shaped defects [2] are known limitation for such direct estimation method. Alternatively, the toughness could be deduced from the mirror constant (Eq. (7), associating Eqs. (3) and ((6)), easier to measure and flaw type independent (not restricted to penny shaped). This expression indicates the flaw size is proportional to r_m.

$$K_{IC} = Y\sigma_f\sqrt{a_c} \text{ or } \sigma_f = \frac{K_{IC}}{Y\sqrt{a_c}} \tag{6}$$

$$B_m = \frac{A_m}{K_{IC}} = \frac{1}{Y}\sqrt{\frac{r_m}{a_c}} \tag{7}$$

Fractographic analysis can finally be used to reveal chemical or thermal residual stresses ($\Delta\sigma$) identifying the ordinate of σ_f versus ${r_m}^{-1/2}$ (Eq. (8)) [9].

$$\sigma_f + \Delta\sigma = \frac{A_m}{\sqrt{r_m}} \tag{8}$$

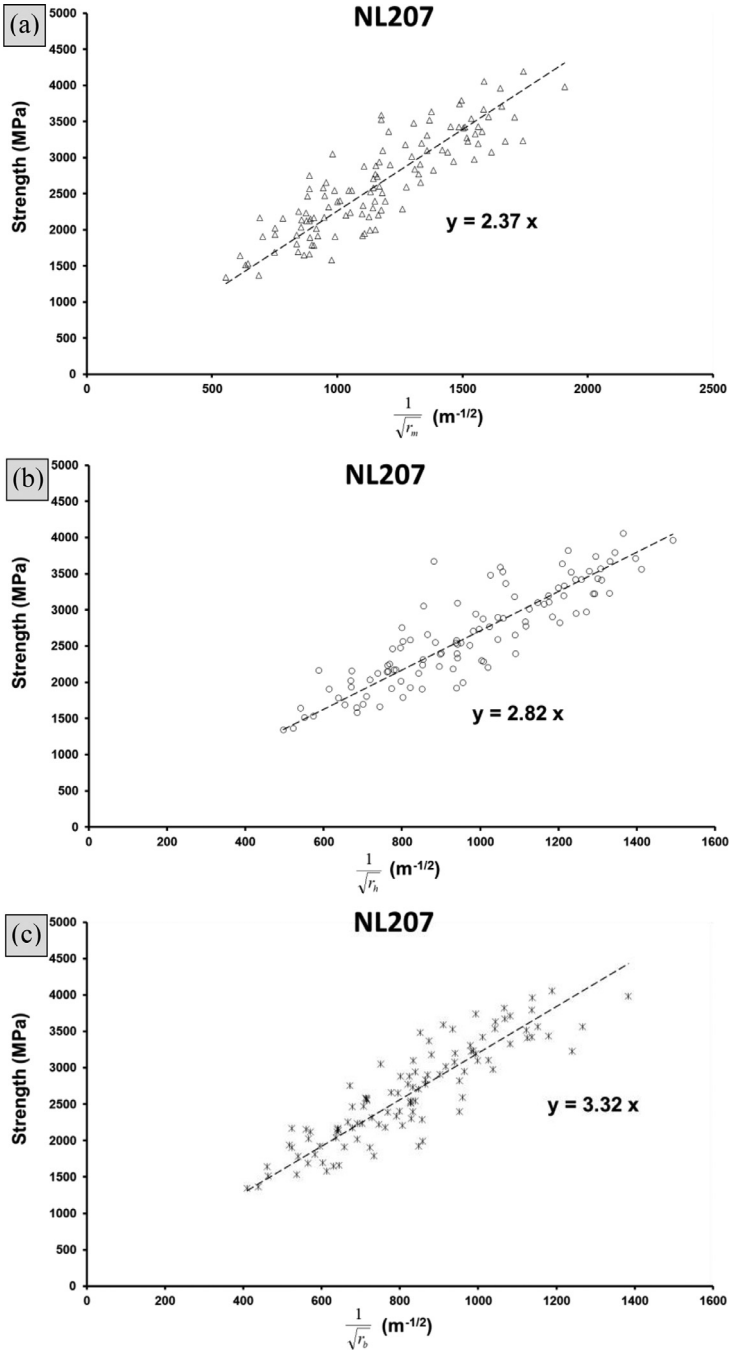

Fig. 14. Tensile strength vs. reciprocal square root of (a). mirror (b). mist (c). hackle outer radius for NL207 fibers.

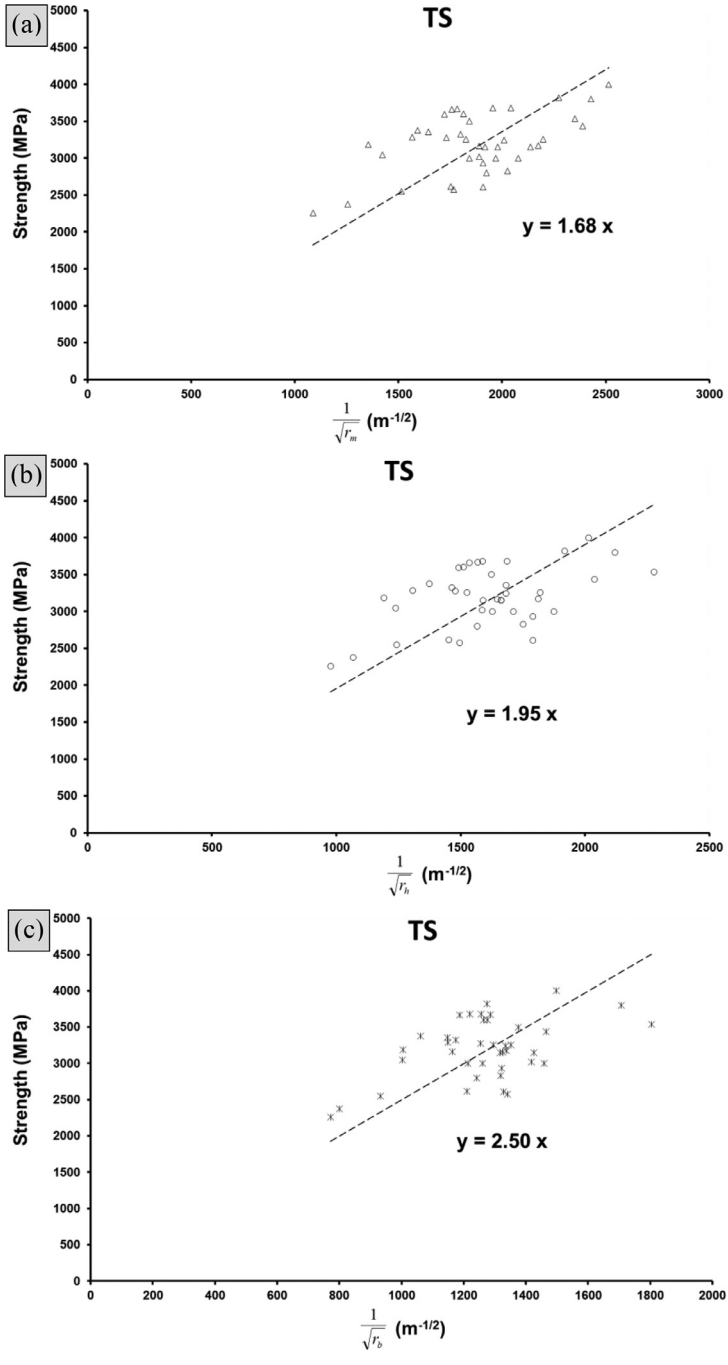

Fig. 15. Tensile strength vs. reciprocal square root of (a). mirror (b). mist (c). hackle outer radius for TS fibers.

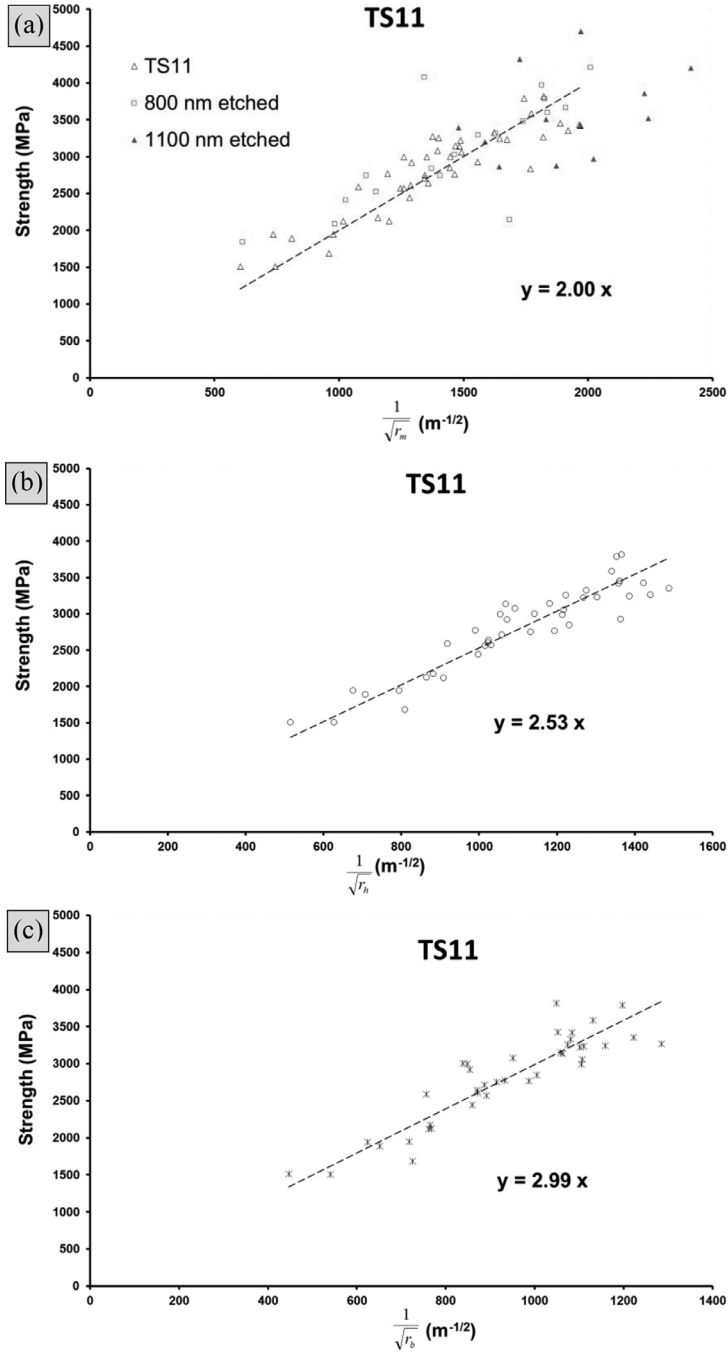

Fig. 16. Tensile strength vs. reciprocal square root of (a). mirror (b). mist (c). hackle outer radius for TS11 fibers. Data for chlorinated TS11 over 800 or 1100 nm are also given.

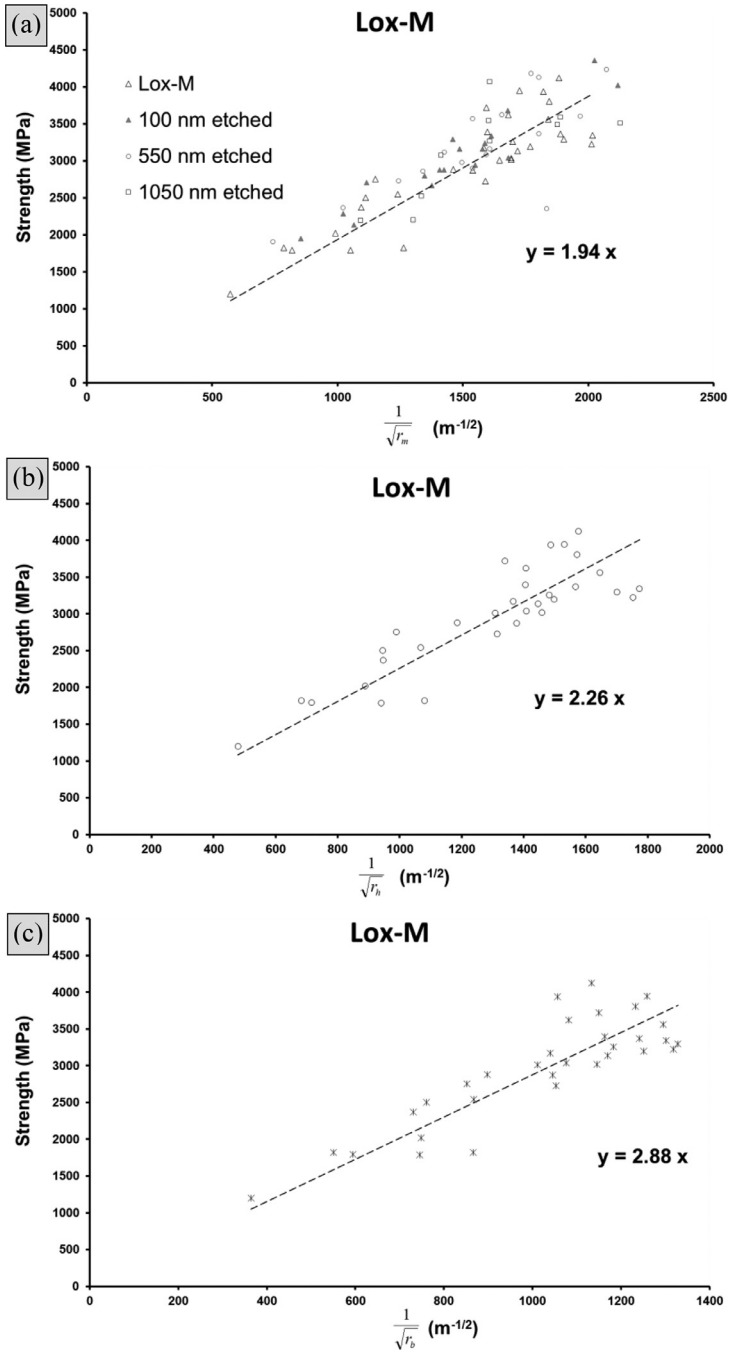

Fig. 17. Tensile strength vs. reciprocal square root of (a). mirror (b). mist (c). hackle outer radius for Lox-M fibers. Data for chlorinated Lox-M over 100 550 or 1050 nm are also given.

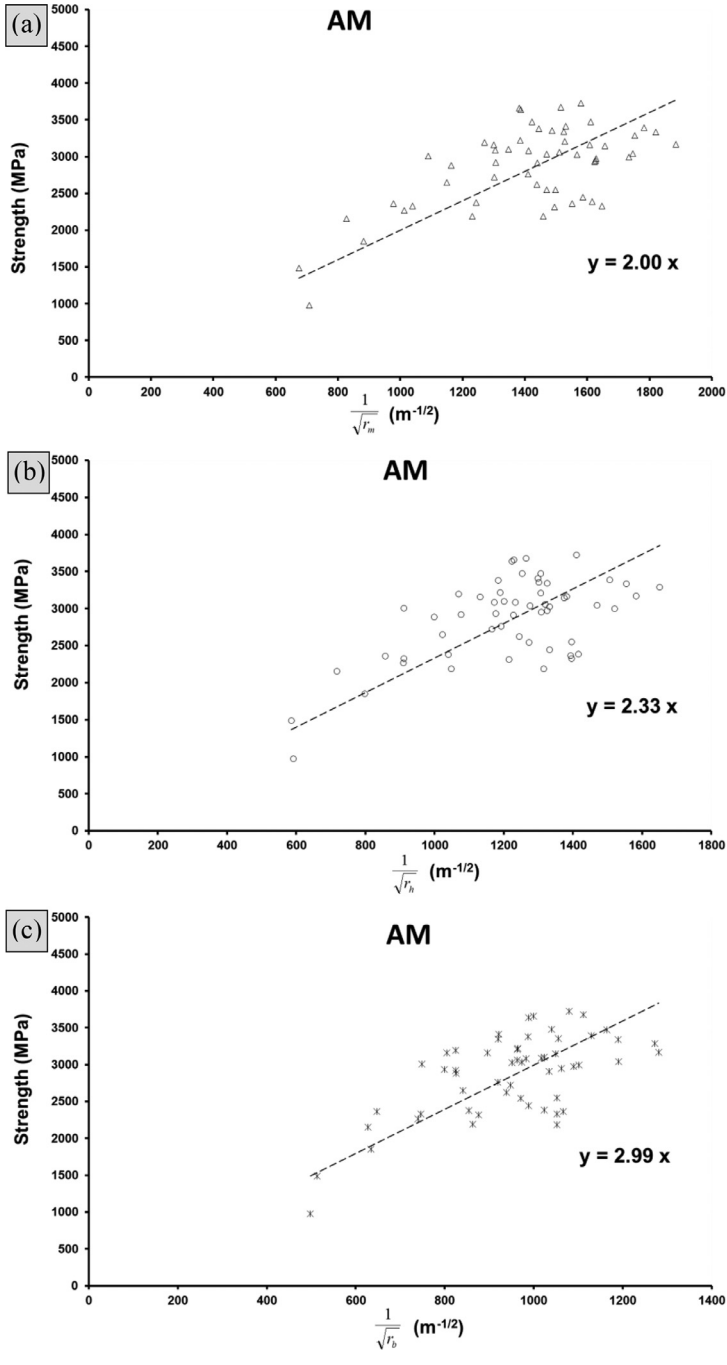

Fig. 18. Tensile strength vs. reciprocal square root of (a). mirror (b). mist (c). hackle outer radius for AM fibers.

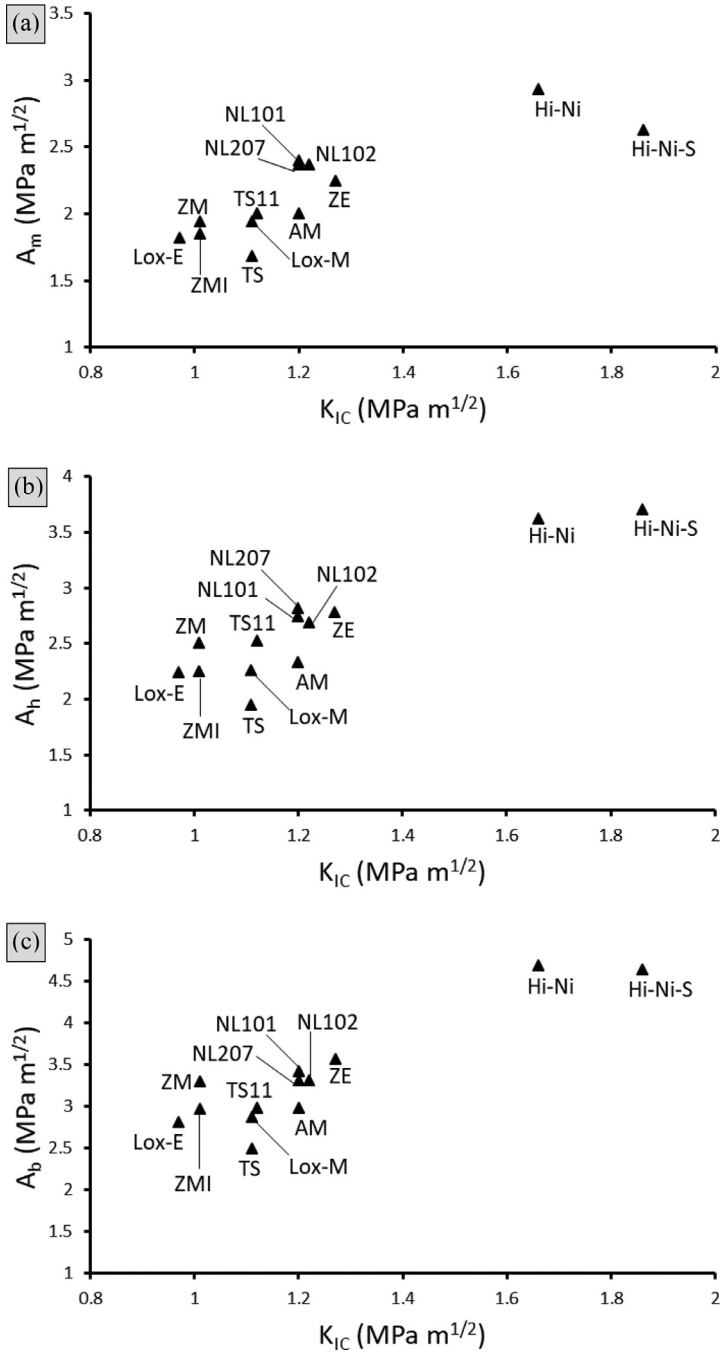

Fig. 19. Relationship between K_{IC} and characteristic stress intensity factors.

Declaration of Competing Interest

The authors declare that they have no known competing financial interests or personal relationships which have, or could be perceived to have, influenced the work reported in this article.

Supplementary Materials

Supplementary material associated with this article can be found in the online version at doi:10.1016/j.dib.2020.106676.

References

[1] F. Teyssandier, G. Puyoo, S. Mazerat, G. Chollon, R. Pailler, F. Babonneau, Contribution to the understanding of the microstructure of first generation Si-C-O fibers, in: M. Halbig, S. Mathur, T. Ohji, M. Singh (Eds.), Advanced Processing and Manufacturing Technologies for Structural and Multifunctional Materials VI, 33, Ceram. Eng. Sci. Proc. Wiley, New York, 2012, pp. 1–11, doi:10.1002/9781118217528.ch1.
[2] S. Mazerat, A. Delcamp, R. Pailler, J. Lamon, H. Plaisantin, Improvement of silicon carbide fibers mechanical properties by Cl2 etching, J. Eur. Ceram. Soc. 38 (16) (2018) 5301–5310, doi:10.1016/j.jeurceramsoc.2018.06.026.
[3] N. Lissart, J. Lamon, Statistical analysis of failure of SiC fibres in the presence of bimodal flaw populations, J. Mater. Sci. 32 (1997) 6107–6117, doi:10.1023/A:1018600119250.
[4] S. Mazerat, A. Delehouze, R. Pailler, Delayed failure prediction of SiC-based bundles: the impact of sampling size, Int. J. Fatigue 138 (2020) 105694, doi:10.1016/j.ijfatigue.2020.105694.
[5] I.J. Davies, T. Ishikawa, Estimation of the fracture toughness of Tyranno Si–Ti–C–O fibres from flaw size and "fracture mirror" data measured in situ a 3-D woven SiC/SiC composite, Int. J. Mater. Prod. Tech. 16 (1–3) (2001) 189–196.
[6] K. Matsunaga, S. Ochiai, K. Osamura, Y. Waku, T. Yamamura, Influence of heat-treatment on mechanical property of Si-Ti-C-O fiber-reinforced aluminum matrix composite, J. Jap. Inst. Metals 57 (1993) 1035–1040, doi:10.2320/jinstmet1952.57.9_1035.
[7] S. Mazerat, R. Pailler, Effect of microstructure and chemical composition on subcritical crack growth in SiC-based fiber tows, Ceram. Int. 47 (2) (2020) 2888–2891, doi:10.1016/j.ceramint.2020.09.052.
[8] S. Mazerat, J. Lacroix, B. Rufino, R. Pailler, Carbon derived from silicon carbide fibers, a comparative study, Mater. Today Com. 19 (2019) 177–185, doi:10.1016/j.mtcomm.2019.01.013.
[9] B.J. Norman, A.C. Jaras, J. Ashall, Measurement of silicon carbide fibre strength in composites from studies of their fracture surfaces, British Ceram. Trans. 92 (2) (1993) 62–66.
[10] G.E. Youngblood, C. Lewinsohn, R.H. Jones, A. Kohyama, Tensile strength and fracture surface characterization of Hi-Nicalon SiC fibers, J. Nucl. Mater. 289 (2001) 1–9, doi:10.1016/S0022-3115(00)00675-9.
[11] T. Morimoto, K. Yamoto, S. Ogihara, The potential strength on an imaginary SiC fiber of optimized diameter and controlled crack sources, in: Proceedings of the SAMPE Symposium, 2005, pp. 713–718.
[12] A.J. Eckel, R.C. Bradt, Strength distribution of reinforcing fibers in a Nicalon fiber/chemically vapor infiltrated silicon carbide matrix composites, J. Am. Ceramic Soc. 72 (3) (1989) 455–458, doi:10.1111/j.1151-2916.1989.tb06152.x.
[13] S. Mazerat, G. Puyoo, G. Chollon, F. Teyssandier, R. Pailler, S. Loison, E. Philippe, Composition and reactivity of various silicon carbide fibers, HTCMC8 Ceram. Trans. 248 (2014) 113–123, doi:10.1002/9781118932995.ch13.
[14] S.R. Choi, J.P. Gyekenyesi, Crack branching and fracture mirror data of glasses and advanced ceramics, NASA 206536 (1998) 1–19.
[15] W.C. Levengood, Effect of origin flaw characteristics on glass strength, J. App. Phys. 29 (1958) 820–827, doi:10.1063/1.1723292.
[16] J.J. Mecholsky, S.W. Freiman, R.W. Rice, Fractographic analysis of ceramics, Am. Soc. Testing Mater. (363–379) (1978), doi:10.1520/STP38101S.
[17] L.C. Sawyer, R. Arons, F. Haimbach, M. Jaffe, K.D. Rappaport, Characterization on Nicalon: strength, structure, and fractography, Ceram. Eng. Surface Proc. 6 (7–8) (1985) 567–575, doi:10.1002/9780470320280.ch9.
[18] L.C. Sawyer, M. Jamieson, D. Brikowski, M.H. Haider, R.T. Chen, Strength, structure, and fracture properties of ceramic fibers produced from polymeric precursors: I, base-line studies, J. Am. Ceram. Soc. 70 (11) (1987) 798–810, doi:10.1111/j.1151-2916.1987.tb05631.x.